SUPPORTING INFORMATION

Multifunctional PVDF Membrane Coated with ZnO-Ag Nanocomposites for Wastewater Treatment and Fouling Mitigation

Xiujuan Chen[a], Wendy Huang[b*], Chunjiang An[c], Renfei Feng[d], Peng Zhang[e]

[a] Department of Civil Engineering, The University of Texas at Arlington, Arlington, Texas, 76019, United States.
[b] Department of Civil Engineering, University of Calgary, Calgary, Alberta, T2N 1N4, Canada
[c] Department of Building, Civil and Environmental Engineering, Concordia University, Montreal, Quebec, Canada H3G 1M8
[d] Canadian Light Source, Saskatoon, S7N 2V3, Canada
[e] Environmental Systems Engineering, University of Regina, Regina, Saskatchewan, Canada S4S 0A2

*corresponding author, phone: +1-306-585-4095; fax: 1-306-585-4855; e-mail: wendy.huang3@ucalgary.ca

Materials and chemicals

PVDF membrane with 0.1 μm of average pore size was purchased from TQX Membrane Technology Ltd. (Xiamen, China). Before modification, the PVDF membrane was cleaned in DI water through ultrasonic treatment at 250 W, 40 KHz for 5 min. ZnO nanoparticles (ZnO NPs, < 100 nm) were purchased from Innochem (Beijing, China). Superoxide dismutase (SOD) typed assay kit and catalase (CAT) assay kit were obtained from Nanjing Jiancheng Bioengineering Institute (Nanjing, China). Chemicals including silver nitrate ($AgNO_3$), sodium borohydride ($NaBH_4$), sodium chloride (NaCl), acrylic acid (AA), 2',7'-Dichlorofluorescin diacetate (DCFH-DA), 1,2-dichloroethane (DCE), diiodomethane and ethylene glycol (EG) were purchased from Sigma-Aldrich (MilliporeSigma Canada Co., Oakville, Canada) with analytical grade and used as received without further purification. Water samples were collected from the secondary wastewater effluent in the Regina Water Treatment Plant, Canada. The *E. coli* concentration was determined to be 10^5 cfu/100 mL through plate count method. The water samples was stored at 4 °C before use.

Characterization of Membrane and ZnO-Ag Nanocomposites

Morphology of membrane surface was characterized by scanning electron microscopy (SEM) (JSM-6510; Rigaku). X-ray photoelectron spectroscopy (XPS) (Kratos AXIS SUPRA; Shimadzu) measurements for nanocomposites and membrane surface were carried out with monochromatic 1486.69 eV Al Kα X-ray source. The zeta potential of membrane surface was determined through an electrokinetic analyzer (SurPASS 3; Anton Paar) with an electrolyte consisting of 1 mM KCl. The crystalline structure of nanocomposites was determined by X-ray diffraction (XRD) (Ultima IV; Rigaku) measurements. The diffraction patterns were recorded in the range of 20° to 90°. The hydroxyl radical ($^{\cdot}$OH) generated by nanocomposites in solution was measured through electron paramagnetic resonance (EPR) (A300; Bruker) spectroscopy. 1.5 μL of dimethylpyridine nitrogen oxide (DMPO) was added in 45 μL of nanocomposites solution (10 wt%). The spectra were obtained after shaken 30 min under conditions of dark and visible light irradiation with xenon lamp. Surface contact angle measurements (OCA20; DataPhysics Instruments) were performed with the sessile drop method. To measure water contact angle, a 5 μL water droplet was dropped on the membrane surface and photographed using a digital camera. To measure under-water oil contact angle, a 10 μL of DCE droplet was dropped on the membrane surface which was immersed in DI water beforehand. To account for variations in the measurements, minimum of three measurements were performed on three different samples at 20 ± 1 °C. Membrane surface energy was calculated with three standard liquids: DI water, EG and diiodomethane.

The Synchrotron-based analyses were carried out in the Canadian Light Source (CLS) at Saskatoon, Canada (Figure S2). The chemical functional groups of nanocomposites and membrane surfaces were studied through Synchrotron-base Attenuated Total Reflection-Fourier Transform Infrared (ATR-FTIR) Spectroscopy and Mapping at the 01B1-01 (Mid-IR) beamline. The FTIR spectra and mappings were acquired with wavenumber ranges of 400 ~ 4000 cm^{-1} and 900 ~ 4000 cm^{-1}, respectively. To compensate atmospheric and

synchrotron ring current changes, background spectrum was taken for each sample. Minimum of five measurements were done for each sample, and the average value was reported. The Synchrotron-based X-ray fluorescence (SR-XRF) measurements were performed at the Very Sensitive Elemental and Structural Probe Employing Radiation from a Synchrotron beamline (VESPERS, 07B2-1). SR-XRF spectra and mappings of Zn and Ag concentration distributions on surfaces of the pristine and modified membranes were measured. The polychromatic X-ray (pink beam) was applied to excite membrane samples, and the emitted XRF spectra were recorded by a four element Vortex® silicon drift detector. The membrane sample was air-dried and cut into small flat sheets (1.0 cm × 1.0 cm) before measurement. The mapping area was 1500 × 150 μm, and the scanning step size was set as 5 μm. The reported XRF spectrum was the average of all spectra from selected mapping area.

Data analysis and QA/QC program

The obtained XPS spectra were processed using XPSPEAKS41 software program. The XRD patterns were analyzed using the MDI Jade 6 software program. FTIR spectra data was processed using the OPUS 7.2 software (Bruker Optics Inc.), and mapping data was analysis using CytoSpec 2.00.01. All the data of contact angle and surface energy was analyzed using SCA20 (DataPhysics Instruments). The SR-XRF data was processed using PyMca 5.5.4, and the processed data was plotted using SigmaPlot 14.0 (Systat Software Inc., San Jose). The quality assurance/quality control (QA/QC) program was followed to ensure the accuracy and reliability of the collected data. To estimate the general membrane characteristics and performances, each experiment was carried out for three different membrane samples which were prepared under the same condition. Each filtration experiment was conducted in duplicate and the average value was reported. All containers were cleaned beforehand with the particular washing liquid for laboratory purposes, and were triply rinsed with DI water and oven dried. All items were sterilized by using an autoclave before contacted with bacteria.

Table S1. Factorial design matrix and the response.

		Factor 1	Factor 2	Factor 3	Response
Std	Run	A: Ag concentration (mM)	B: Sintering temperature (ºC)	C: Light condition	CFU (% of control)
1	9	6	60	0	31.91
2	5	6	60	0	29.63
3	3	8	60	0	23.48
4	15	8	60	0	25.75
5	13	6	450	0	8.48
6	12	6	450	0	8.32
7	6	8	450	0	5.97
8	7	8	450	0	6.03
9	2	6	60	1	21.1
10	16	6	60	1	19.15
11	4	8	60	1	14.98
12	10	8	60	1	17.48
13	11	6	450	1	6.37
14	14	6	450	1	6.03
15	1	8	450	1	3.17
16	8	8	450	1	3.23

Table S2: Analysis of variance (ANOVA)

Source	Sum of Squares	df	Mean Square	F Value	p-value Prob > F	
Model	1413.30	6	235.55	172.06	< 0.0001	significant
A-Ag concentration	59.68	1	59.68	43.59	< 0.0001	
B-Sintering temperature	861.07	1	861.07	628.97	< 0.0001	
C-Light condition	107.65	1	107.65	78.63	< 0.0001	
AB	5.41	1	5.41	3.95	0.0782	
AC	0.69	1	0.69	0.50	0.4961	
BC	49.21	1	49.21	35.95	0.0002	
Residual	12.32	9	1.37			
Lack of Fit	2.04	1	2.04	1.59	0.2426	not significant
Pure Error	10.28	8	1.28			
Cor Total	1425.62	15				

The Model F-value of 172.06 implies the model is significant. There is only a 0.01% chance that an F-value this large could occur due to noise.

Values greater than 0.1000 indicate the model terms are not significant. "Values of ""Prob > F"" less than 0.0500 indicate model terms are significant. " In this case A, B, C, BC are significant model terms.

"The ""Lack of Fit F-value"" of 1.59 implies the Lack of Fit is not significant relative to the pure" "error. There is a 24.26% chance that a ""Lack of Fit F-value"" this large could occur due" to noise. Non-significant lack of fit is good -- we want the model to fit.
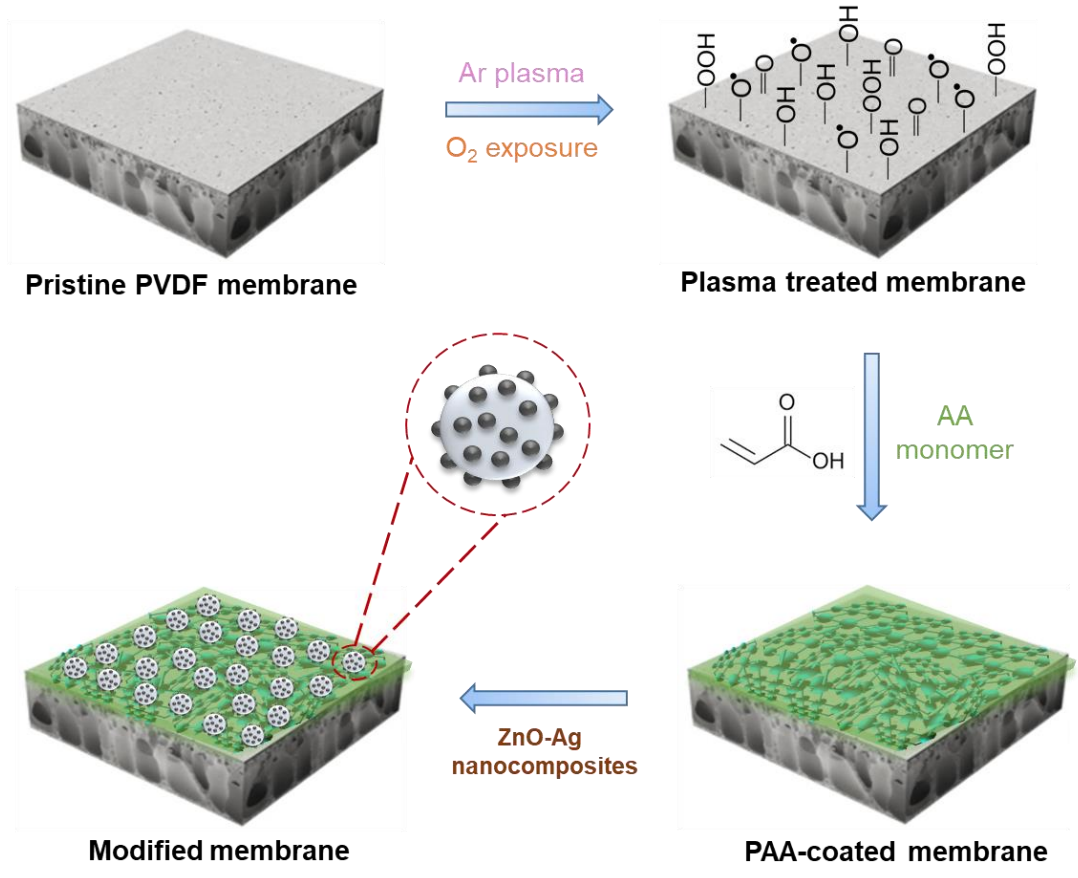
Figure S1. Schematic illustration of membrane functionalization.
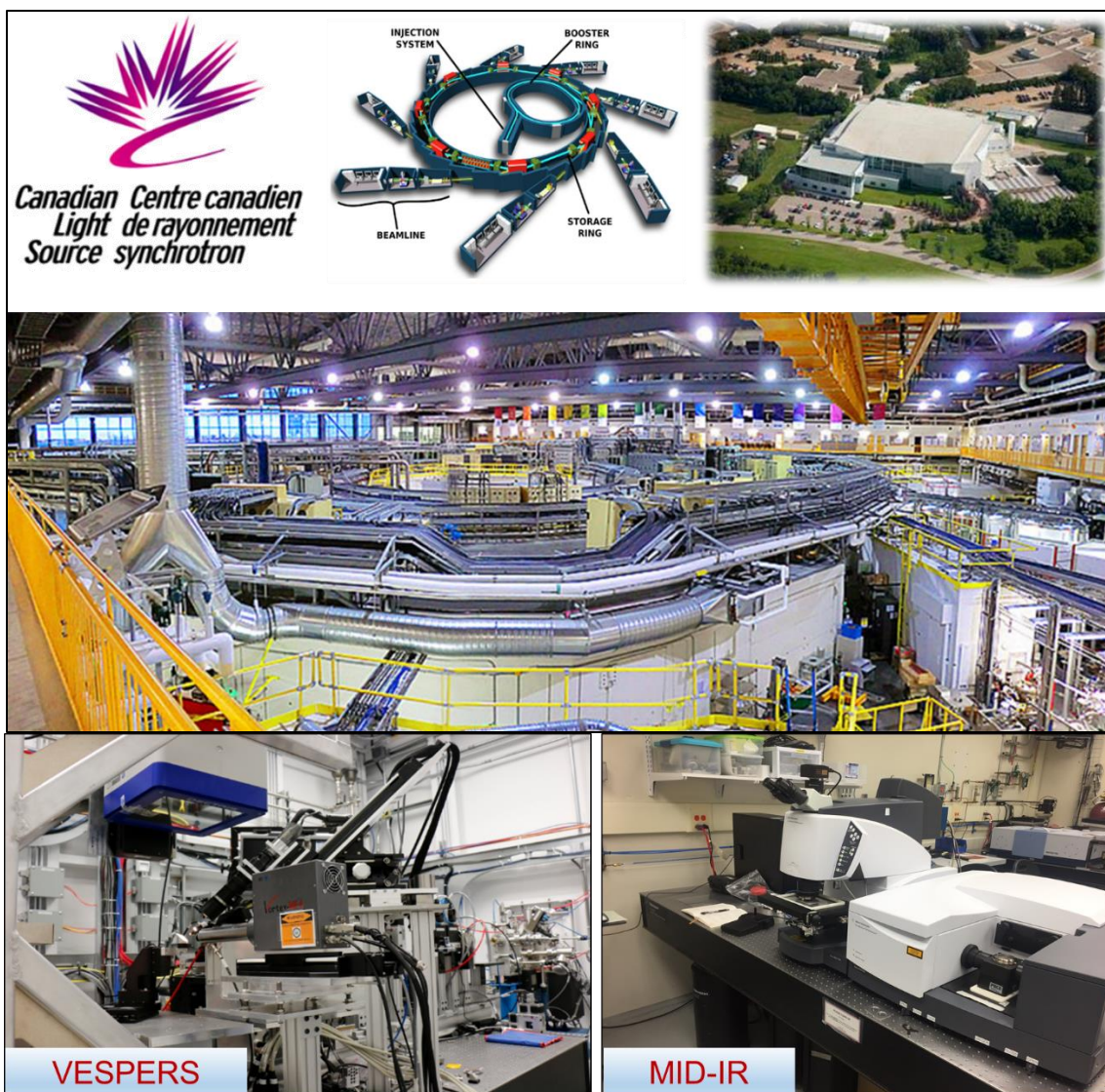
Figure S2. Canadian light source, synchrotron beamline stations of Very Sensitive Elemental and Structural Probe Employing Radiation from a Synchrotron (VESPERS) and Mid Infrared Spectromicroscopy (MID-IR). (http://www.lightsource.ca/).
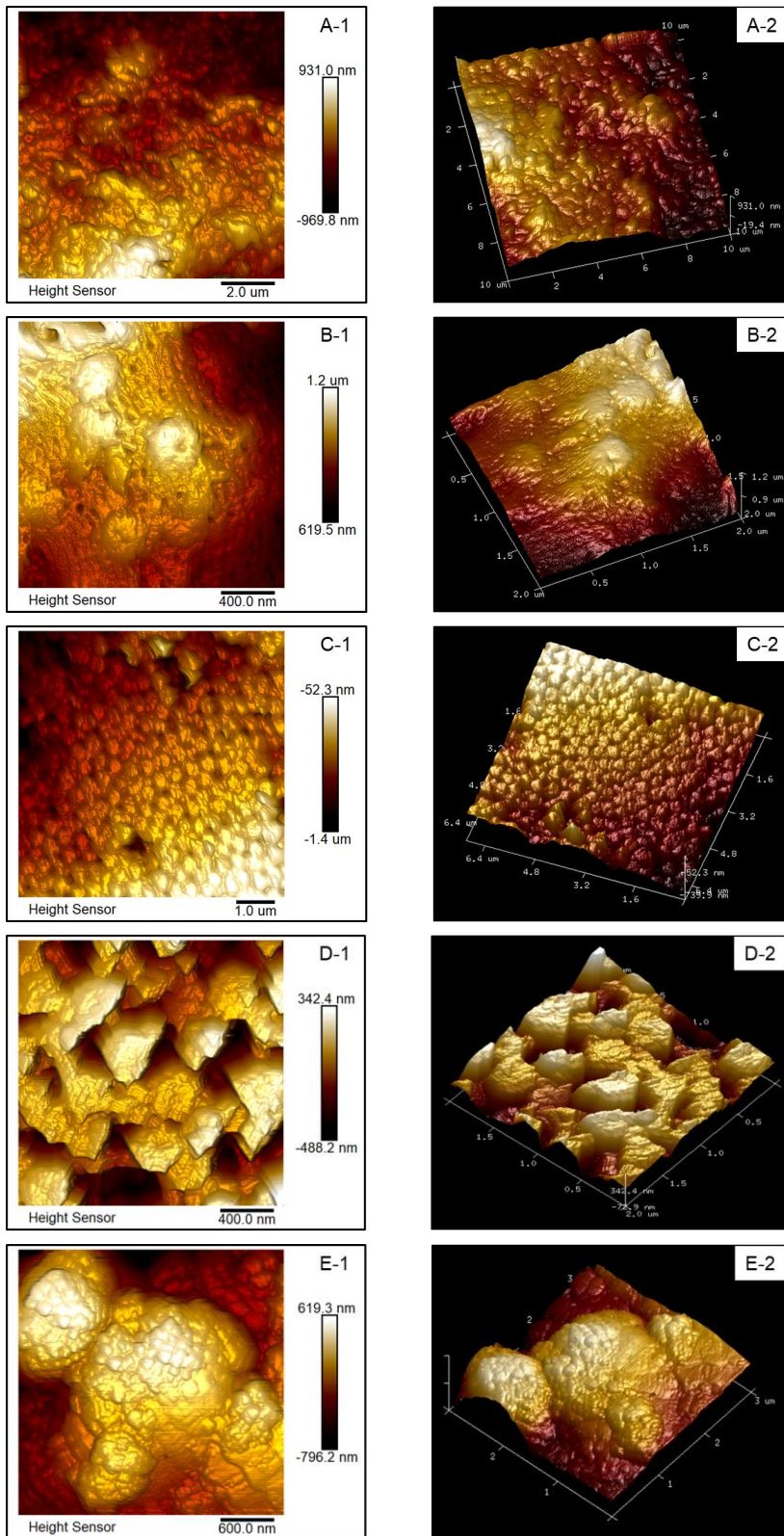
Figure S3. AFM images of membrane surfaces: (A) – (B) pristine PVDF membrane (Ra = 120 nm), (C) – (D) PAA-coated membrane (Ra = 100 nm), and (E) ZnO-7Ag modified membrane (Ra = 191 nm).
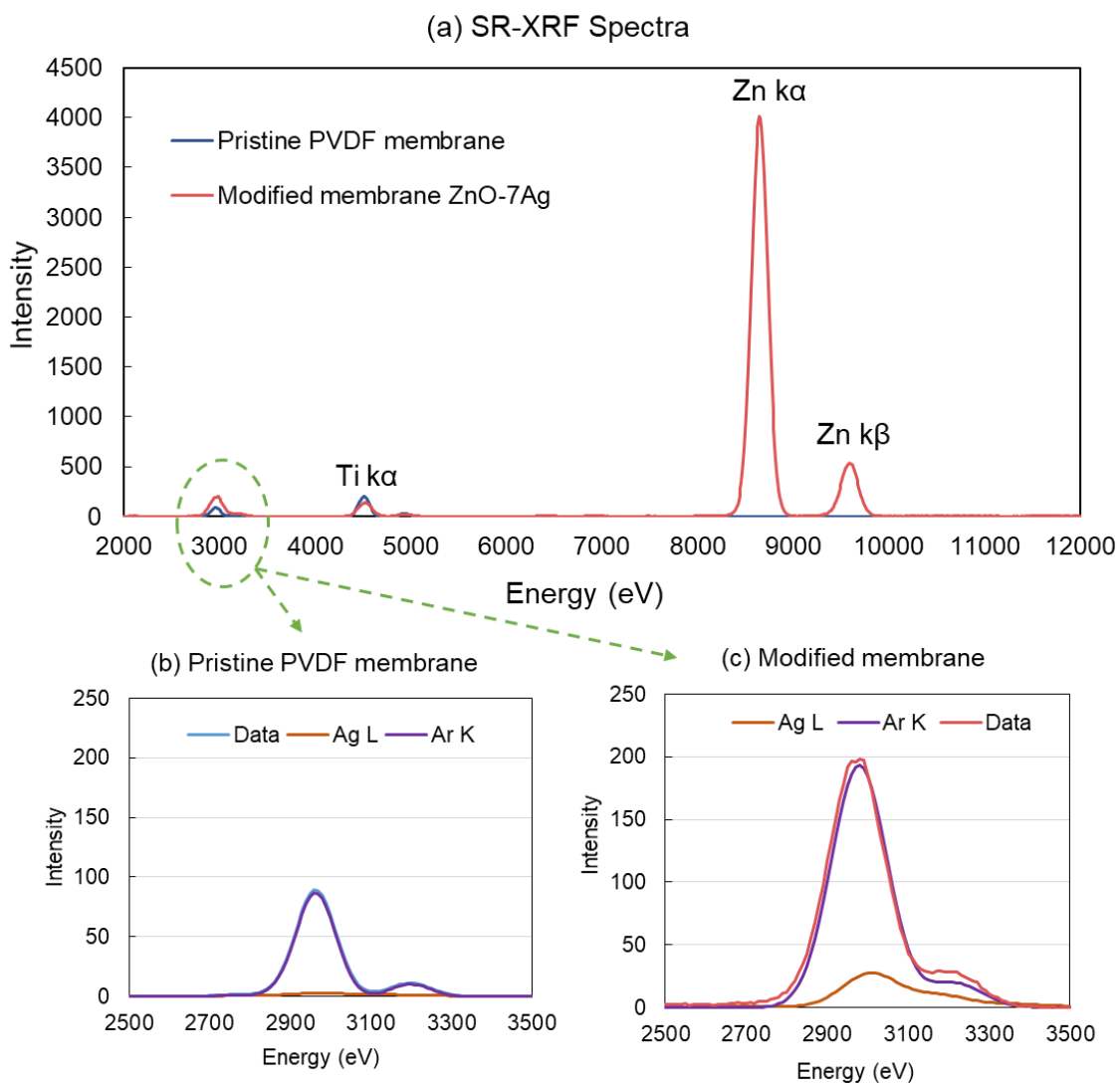
Figure S4. (a) SR-XRF spectra from membrane surfaces, (b) fitted SR-XRF spectrum from pristine PVDF membrane surface, and (c) fitted SR-XRF spectrum from modified membrane surface.
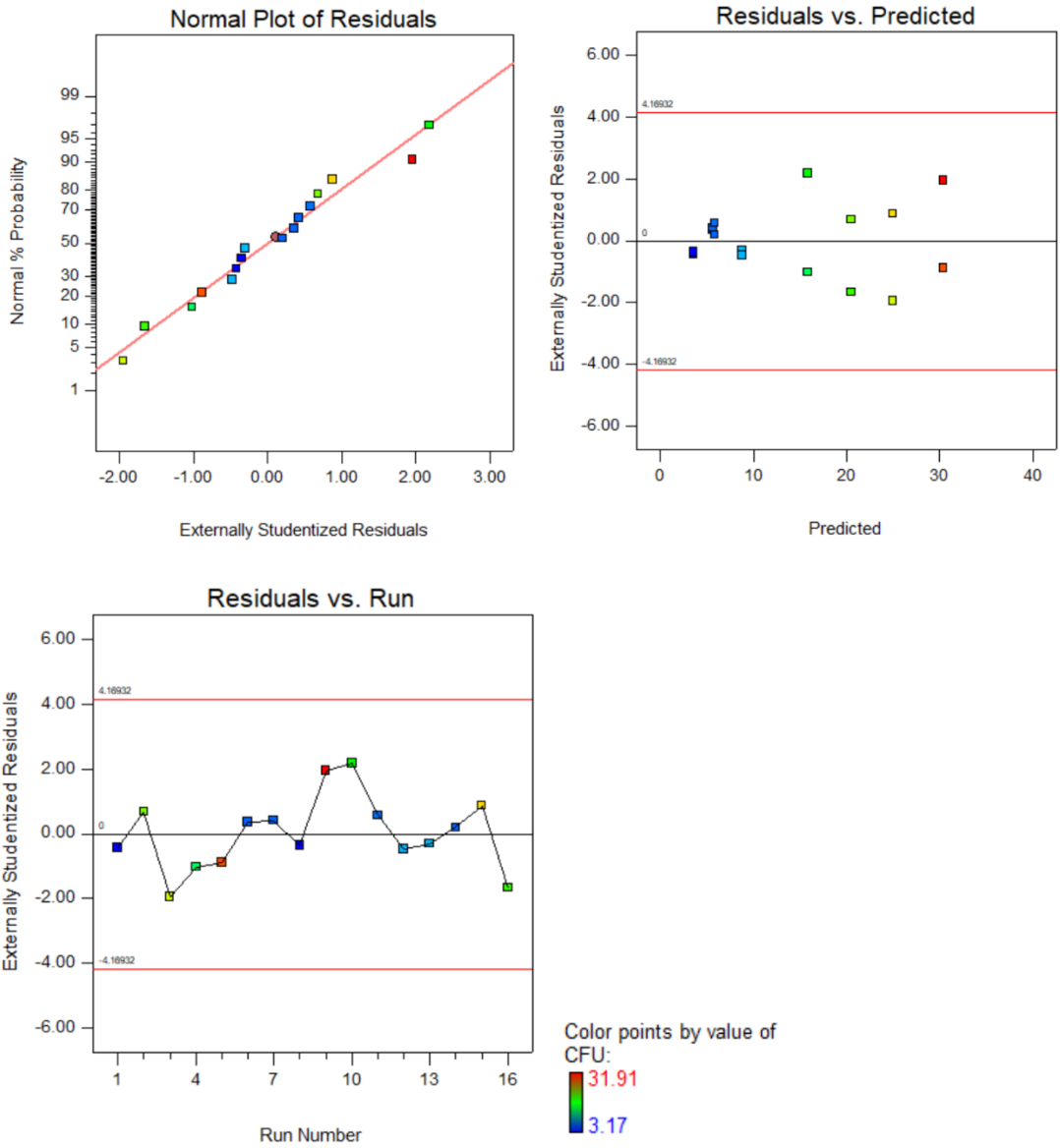
Figure S5. Verification of assumptions for ANOVA.

(a) Normal plot
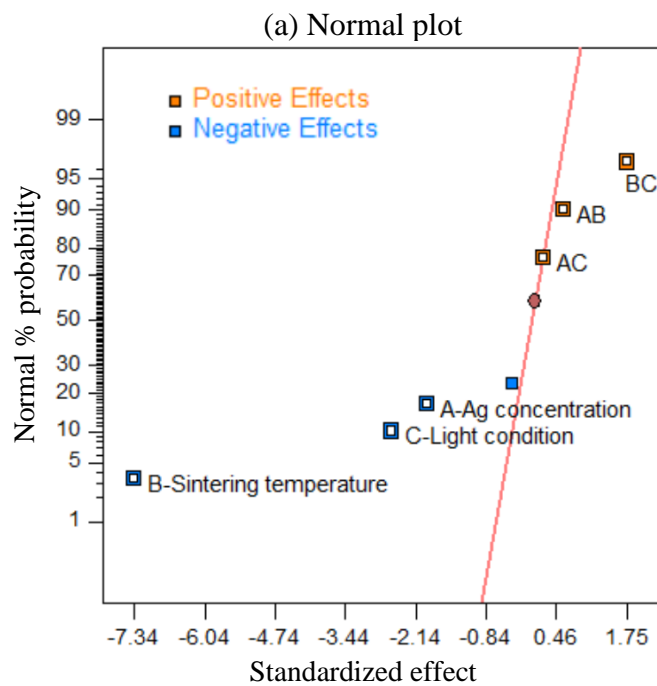
(b) Standardized effects and their contributions

Term	Standardized Effect	Sum of Squares	% Contribution
A-Ag concentration	-1.93	59.68	5.44
B-Sintering temperature	-7.34	861.07	78.56
C-Light condition	-2.59	107.65	9.82
AB	0.58	5.41	0.49
AC	0.21	0.69	0.063
BC	1.75	49.21	4.49

Figure S6. Normal plot of standardized effects (a), and their contributions (b).
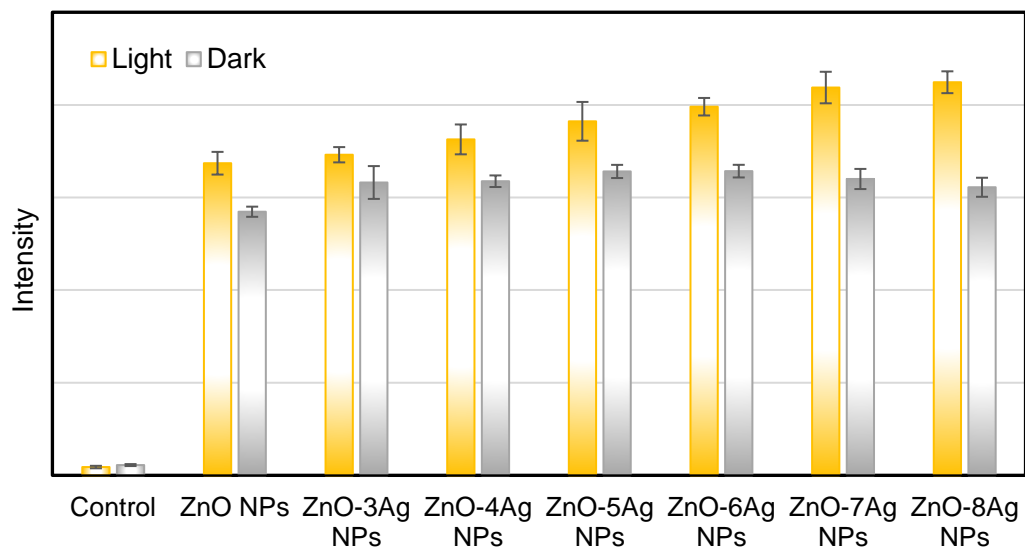
Figure S7. Relative fluorescence intensity of intracellular ROS after 3 h of contact with nanoparticles. The fluorescence intensity of *E. Coli* after 3 h of contact with DCFH-DA without nanoparticles was used as control.
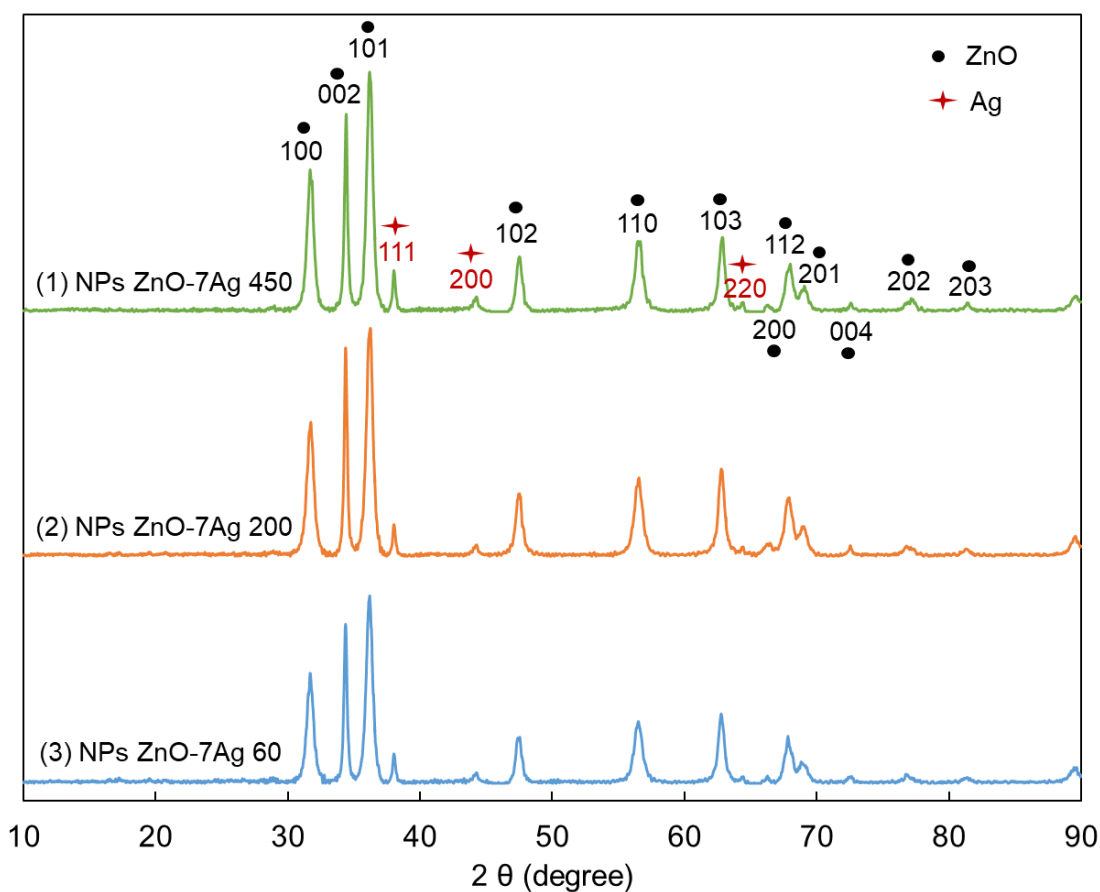
Figure S8. XRD patterns of ZnO-7Ag nanocomposites obtained under different temperatures.

The diffraction peaks at 2θ = 31.8°, 34.4°, 36.3°, 47.5°, 56.6°, 62.9° and 67.9° were corresponding to the (100), (002), (101), (102), (110), (103) and (112) crystal planes of wurtzite structure of ZnO. The diffraction peak at 2θ = 38.11° corresponded to the (111) crystal planes of metallic Ag. There were two additional peaks (at 2θ = 44.28° and 64.43°) also assigned to metallic Ag, suggesting the formation of Ag entities as second phase clusters (Yıldırım et al., 2013). No diffraction peaks at 34.2° for Ag_2O was observed, which might be due to the low amount of Ag_2O in all samples (Zhang et al., 2008).
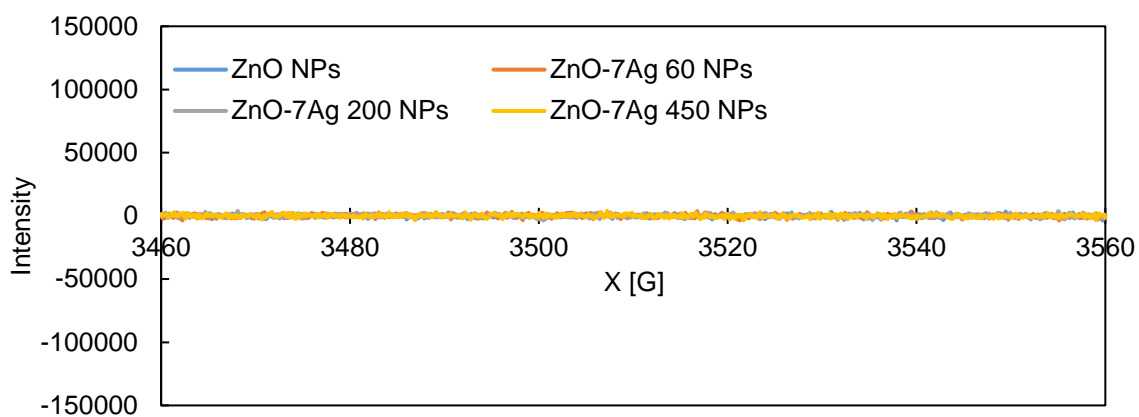
Figure S9. EPR spectra of ZnO NPs and ZnO-7Ag nanocomposites after 30 min under dark condition. There was no obvious signal observed for all samples.

(a)

Pristine PVDF membrane
1405
Modified membrane ZnO-3Ag
1590
Modified membrane ZnO-4Ag
1650
Modified membrane ZnO-5Ag
Modified membrane ZnO-6Ag
Modified membrane ZnO-7Ag
Modified membrane ZnO-8Ag
1377
1180

Wavenumber (cm^{-1})

(b)

ZnO NPs
ZnO-3Ag NPs
ZnO-4Ag NPs
ZnO-5Ag NPs
ZnO-6Ag NPs
ZnO-7Ag NPs
ZnO-8Ag NPs

Wavenumber (cm^{-1})
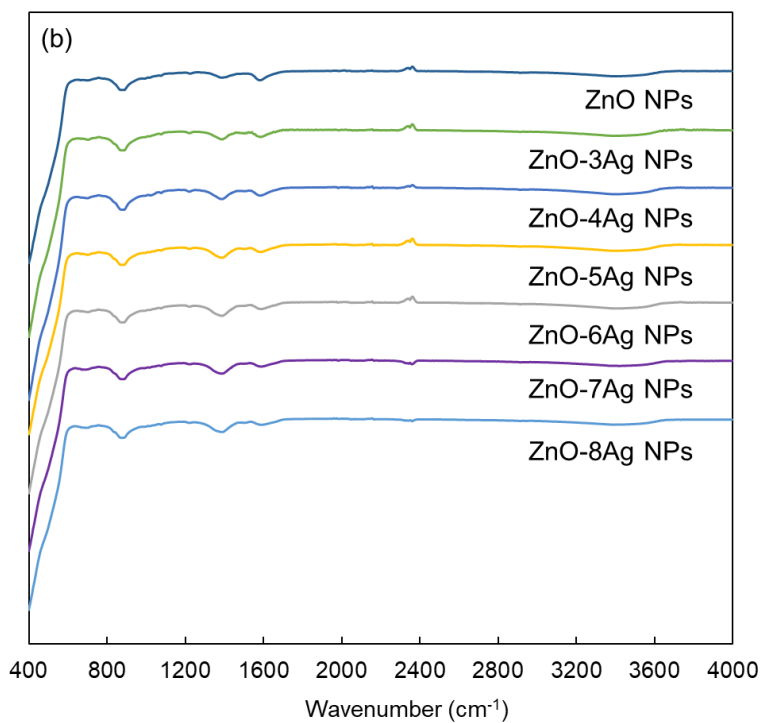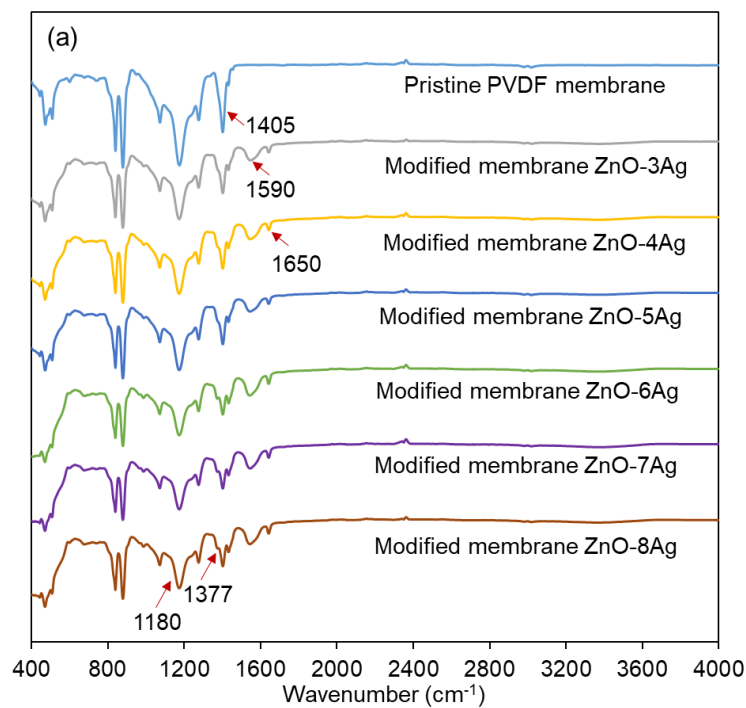
Figure S10. ATR-FTIR spectra of membrane surfaces, ZnO NPs and ZnO-7Ag nanocomposites.

15
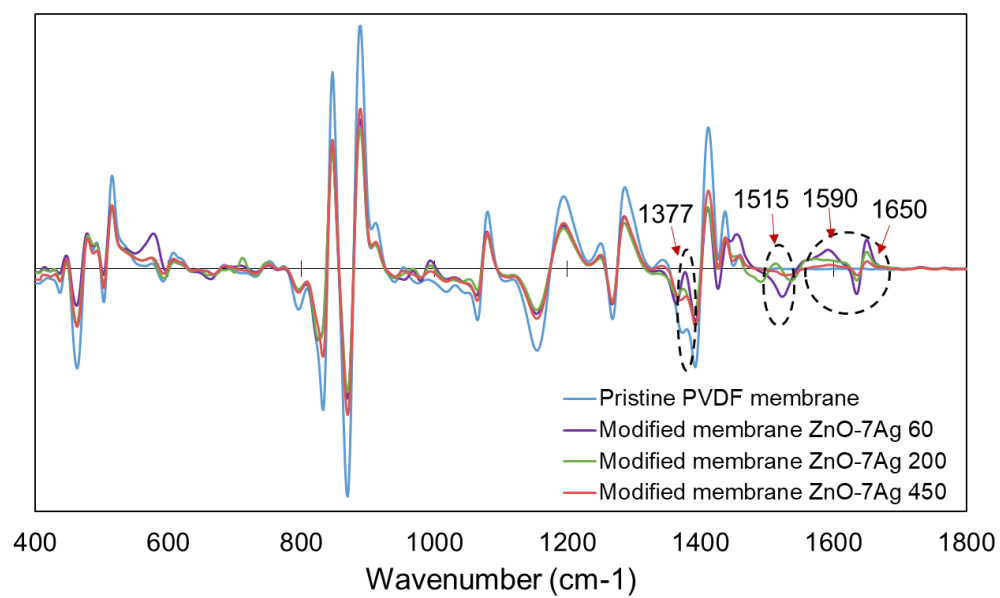
Figure S11. Second derivative ATR-FTIR spectra of membrane surfaces.
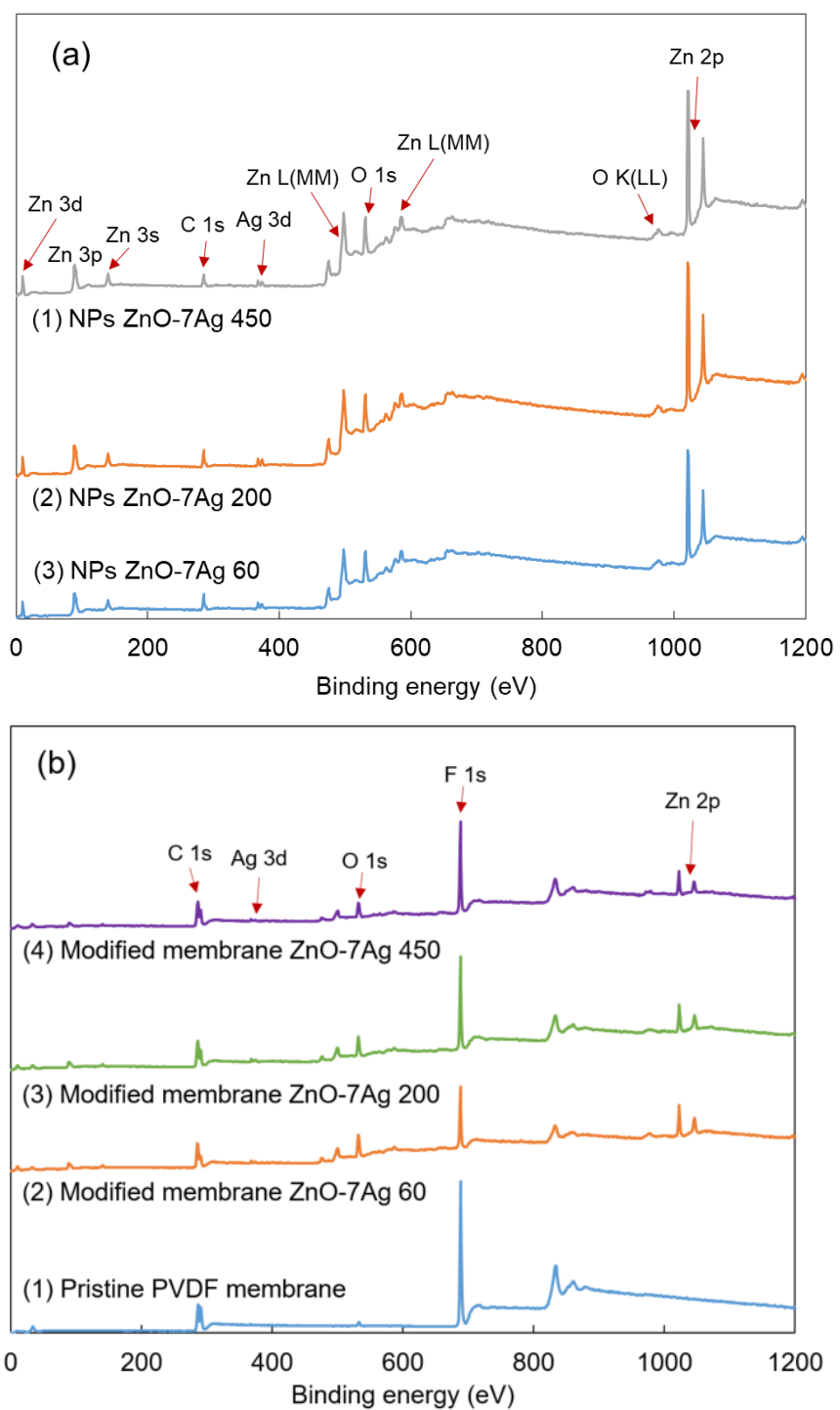
Figure S12. XPS wide-scan spectra of (a) ZnO-7Ag nanocomposites obtained under different temperatures, and (b) the pristine PVDF and modified membrane surfaces.
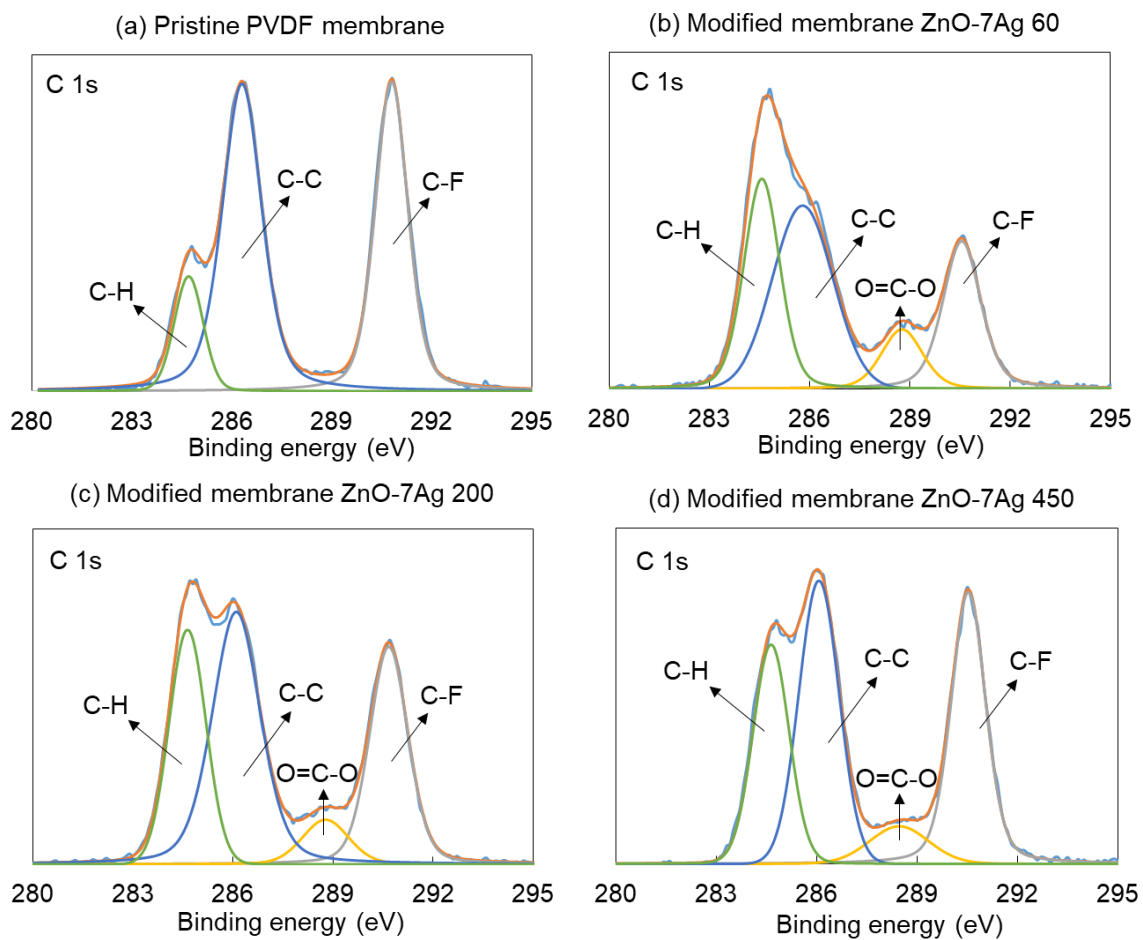
Figure S13. C 1s XPS spectra of the pristine PVDF and modified membrane surfaces.
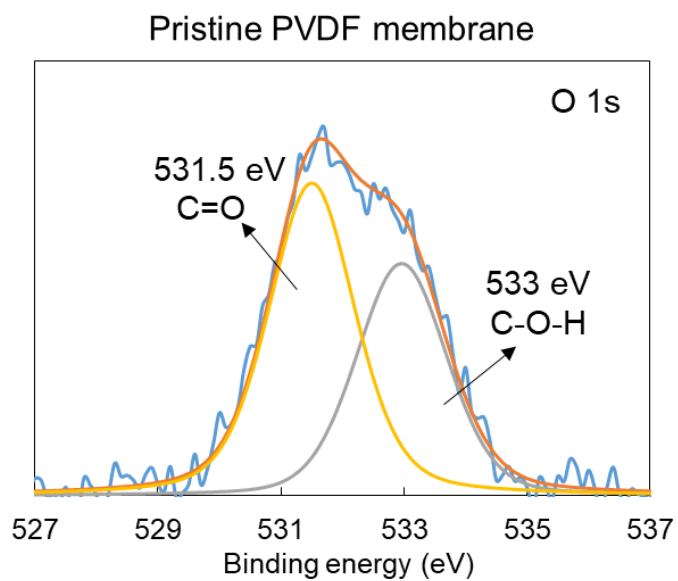
Figure S14. O 1s XPS spectra of the pristine PVDF membrane surface.

Reference

Zhang, H., Wang, G., Chen, D., Lv, X. and Li, J., 2008. Tuning photoelectrochemical performances of Ag - TiO2 nanocomposites via reduction/oxidation of Ag. Chemistry of Materials. 20(20), 6543-6549.

Yıldırım, Ö.A., Unalan, H.E. and Durucan, C., 2013. Highly efficient room temperature synthesis of silver-doped zinc oxide (ZnO:Ag) nanoparticles: Structural, optical, and photocatalytic properties. Journal of the American Ceramic Society. 96(3), 766-773.